Journal of Biomechanics 89 (2019) 128–133

Contents lists available at ScienceDirect

Journal of Biomechanics

journal homepage: www.elsevier.com/locate/jbiomech
www.JBiomech.com

Short communication

Analysis of forearm rotational motion using biplane fluoroscopic intensity-based 2D–3D matching

Shingo Abe [a,c], Yoshito Otake [b], Yusuke Tennma [b], Yuta Hiasa [b], Kunihiro Oka [a], Hiroyuki Tanaka [a], Atsuo Shigi [a], Satoshi Miyamura [a], Yoshinobu Sato [b], Tsuyoshi Murase [a,*]

[a] Department of Orthopaedic Surgery, Osaka University Graduate School of Medicine, 2-2 Yamadaoka, Suita, Osaka 565-0871, Japan
[b] Nara Institute of Science and Technology, 8916-5 Takayama, Ikoma, Nara 630-0192, Japan
[c] Toyonaka Municipal Hospital, 4-14-1 Shibahara, Toyonaka, Osaka 560-8565, Japan

ARTICLE INFO

Article history:
Accepted 11 April 2019

Keywords:
Motion analysis
Forearm rotational motion
Intensity-based 2D–3D matching
Biplane fluoroscopy
Automatic registration

ABSTRACT

Measuring three-dimensional (3D) forearm rotational motion is difficult. We aimed to develop and validate a new method for analyzing 3D forearm rotational motion. We proposed biplane fluoroscopic intensity-based 2D–3D matching, which employs automatic registration processing using the evolutionary optimization strategy. Biplane fluoroscopy was conducted for forearm rotation at 12.5 frames per second along with computed tomography (CT) at one static position. An arm phantom was embedded with eight stainless steel spheres (diameter, 1.5 mm), and forearm rotational motion measurements using the proposed method were compared with those using radiostereometric analysis, which is considered the ground truth. As for the time resolution analysis, we measured radiohumeral joint motion in a patient with posterolateral rotatory instability and compared the 2D–3D matching method with the simulated multiple CT method, which uses CTs at multiple positions and interpolates between the positions. Rotation errors of the radius and ulna between these two methods were 0.31 ± 0.35° and 0.32 ± 0.33°, respectively, translation errors were 0.43 ± 0.35 mm and 0.29 ± 0.25 mm, respectively. Although the 2D–3D method could detect joint dislocation, the multiple CT method could not detect quick motion during joint dislocation. The proposed method enabled high temporal- and spatial-resolution motion analyses with low radiation exposure. Moreover, it enabled the detection of a sudden motion, such as joint dislocation, and may contribute to 3D motion analysis, including joint dislocation, which currently cannot be analyzed using conventional methods.

1. Introduction

Forearm supination/pronation is crucial for daily activities (Morrey et al., 1981). Osseous stability of normal elbow joints differs with forearm rotational position (Omori et al., 2016). Posterolateral rotatory instability (PLRI) of the elbow is characterized by elbow instability depending on the forearm's rotational position (O'Driscoll et al., 1991). Accurate evaluation of dynamic forearm rotation is necessary to understand PLRI pathology. Conventional fluoroscopic motion analysis is limited to two-dimensional (2D) analysis of in vivo motion (Stiehl et al., 1997). However, forearm rotational motion comprises not only 2D motion but also three-dimensional (3D) motion (Tay et al., 2010). Although multiple position computed tomography (multiple CT) (Abe et al., 2018; Tay et al., 2008) can analyze 3D motion by interpolation using computer software, it increases radiation exposure, procedure time, and medical costs. Because we did not dynamically capture the image using multiple CT in this study, the data generated could not be used to analyze rapid motions such as joint dislocation.

We hypothesized that 2D–3D matching of fluoroscopy, which provides high temporal resolution, and CT, which provides high spatial resolution, would enable accurate 3D motion analysis with minimal radiation exposure. Biplane fluoroscopic intensity-based matching reportedly improves matching accuracy compared with single plane feature-based matching (Hunsche et al., 2017; Massimini et al., 2011; Otake et al., 2013; Zhu et al., 2012). A previous feature-based 2D–3D method enabled manually moving the target bone within virtual fluoroscopic images until the projected silhouettes aligned with the segmented contour on image planes (Massimini et al., 2011). We developed a biplane fluoroscopic intensity-based 2D–3D method using an automatic matching program, which could avoid complicated manual procedures. We aimed to validate the proposed 2D–3D matching method by

* Corresponding author.
E-mail address: tmurase-osk@umin.ac.jp (T. Murase).

https://doi.org/10.1016/j.jbiomech.2019.04.017
0021-9290/

analyzing forearm rotational motion and measuring radiation exposure. We compared captures of the rapid motion of the radiohumeral joint in a PLRI patient using 2D–3D and simulated multiple CT methods.

2. Material and methods

The study was approved by our institutional review board (approval no. 15521-2).

2.1. Biplane fluoroscopic imaging system and dynamic forearm rotation data

A biplane C-arm (Allura Clarity FD20/20, Philips Healthcare, The Netherlands), which acquires X-ray images in both the anterior–posterior and lateral directions, was used (Fig. 1). Testing conditions were as follows: frames per seconds: 12.5; field-of-view (FOV): 378 × 378 mm with an image resolution of 1024 × 1024 pixels (pixel size: 0.37 mm) in anterior–posterior view and 292 × 292 mm with 1024 × 1024 pixels (pixel size: 0.29 mm) in lateral view; and output power "auto" because tube voltage or tube current was not manually adjustable in this equipment. To maintain synchronicity between the biplane images, the C arm alternated X-ray radiation in the anterior–posterior and lateral directions every 40 ms at 12.5 fps. The C-arm controls X-ray tube parameters, kV, mA, and/or exposure time such that the required dose or dose rate is determined by the entrance plane of image detector. The C-arm is equipped with flat panel detectors that can minimize image distortion. The anterior–posterior and lateral sets of X-ray sources and detectors were perpendicularly positioned. Before the testing procedure, we acquired biplane images of a calibration box designed such that the distance between its corners was 11 cm to calculate the relative position of the two X-ray sources and distance between the X-ray sources and detector (Kato and Billinghurst, 1999). Hence, we set the global coordinate system in the biplane equipment. For validation study, we manufactured an entire arm phantom (Fig. 2; Kyoto Kagaku Co. Ltd, Kyoto, Japan). The palmar side of the phantom was set upward on the anterior view at the initial frame and manually rotated approximately 360° (twice of 0°–90°–0°) using a goniometer at a rate of approximately 40°/s for 10 s (125 images in each anterior-posterior and lateral views). Because the previous study reported that the required range of motion of forearm rotation was 60–120° for daily living activities (Aizawa et al., 2010), we set the range at 40°/s to cover these daily activities in 3 s. The resulting rotation speed was not completely constant due to manual rotation. We practiced the motion until we could naturally move the phantom within the FOV and recorded one cycle. We performed the same experiment on a different day and acquired two data sets. The two one-sided test (TOST) was performed, and the 95% CI of the mean difference between trial 1 and 2 was described to assess repeatability. For in vivo forearm rotational analysis, a PLRI patient manually rotated the forearm from full pronation toward full supination with examiner assisting extension and axial compression and then back toward full pronation (~360°) for approximately 5 s.

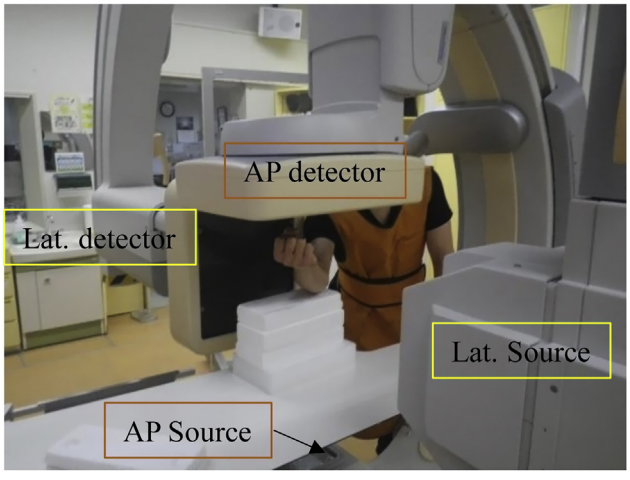

Fig. 1. The biplane C-arm is shown. The participant set his forearm on the scanning range of the C-arm. Lateral (Lat.) and anterior-posterior (AP) sources and detector are shown.

2.2. CT and static data of the forearm

Low-dose CT scanning mode (Oka et al., 2009) of one of two CT equipments (Aquilion One, Toshiba, Japan; Optima CT 660, GE Healthcare, USA) was used on the phantom and patient forearm with the following conditions: slice intervals: 1.25 mm; tube voltage: 120 kV; tube current: 10 mA; and helical pitch: 0.562:1. Segmentation and reconstruction of bone surface models were conducted with the commercial software Bone viewer (Orthree Co., Ltd, Osaka, Japan). The system-reported accuracy of the bone model was 0.46 mm (Oka et al., 2009).

2.3. Biplane fluoroscopic intensity-based 2D–3D matching method (2D–3D method)

Fluoroscopy was performed to obtain dynamic information, and CT was used to obtain 3D static information. Intensity-based 2D–3D matching calculates the 3D position of the target bone during forearm rotation based on image pixel intensity. To remove strong gradients in 2D and 3D images caused by the stainless-steel spheres in the phantom, the spheres were erased using the inpainting technique (Li, 2011) (Fig. 3). The proposed method employs automatic matching using evolutionary optimization (Otake et al., 2013), processed by MATLAB (The Mathworks Inc., Natick, MA, USA). Evolutionary optimization is characterized by its robustness against incorrect local optimum, resulting in a better convergence to the correct matching despite large initialization errors. Evolutionary optimization searches for optimum transformation in successive stages called *generations*. In each generation, the algorithm generates multiple hypotheses (i.e., transformations) and evaluates their goodness by computing the similarity between the fluoroscopic findings and digitally reconstructed radiograph (DRR) generated from CT and the transformation, which is used to generate better hypotheses in the next generation. The initial bone position in the first frame was set by manual matching; matching of the bone was automatically calculated for the subsequent frames using the calculated value of the former frame as the initial value. Six degrees-of-freedom (6 DOF) were calculated for the rotation and translation of the bones for all frames in the global coordinate system.

2.4. Radiostereometric analysis (RSA)

To compare the results of the 2D–3D method with the ground truth, we employed RSA, (de Bruin et al., 2008). RSA uses ray trace intersections of implanted stainless-steel spheres to determine the 3D spatial position of the bone. The quaternion algorithm (Horn, 1987) was used for pose estimation by RSA. Six DOF were calculated for the rotation and translation of bones in the global coordinate system.

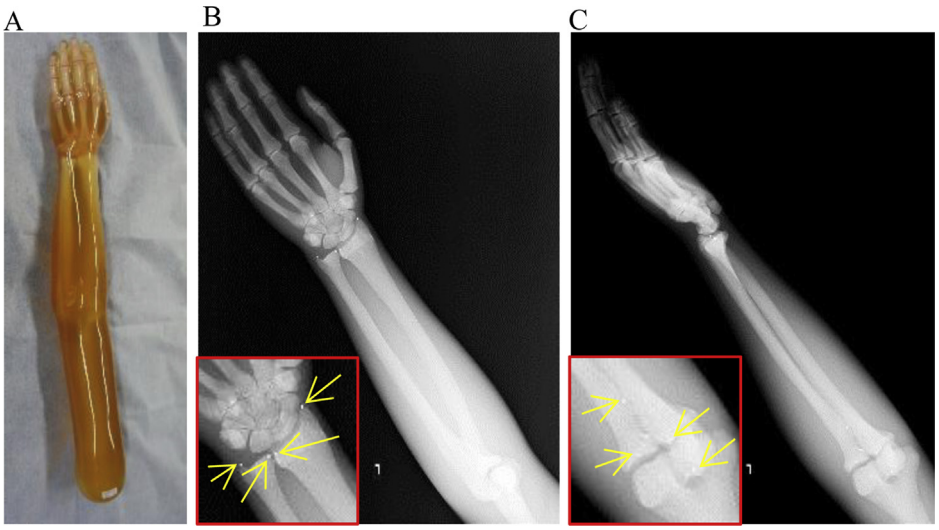

Fig. 2. An entire arm phantom with bones ($CaCO_3$/$BaSO_4$/epoxy resin; 350 Hounsfield Unit [HU]), soft tissue (polyurethane; 0 HU), and four stainless steel spheres (diameter, 1.5 mm) implanted on anatomical landmarks of the radius and ulna were manufactured (Kyoto Kagaku Co. Ltd, Kyoto, Japan). (a) Photograph of the arm phantom, (b) anteroposterior x-ray view, and (c) lateral x-ray view. Yellow arrows indicate the position of the stainless steel spheres. (For interpretation of the references to colour in this figure legend, the reader is referred to the web version of this article.)

2.5. Phantom motion comparison between the 2D–3D method and RSA

Euler angles were used to compare 6 DOF for the rotation and translation of the bones between the proposed 2D–3D method and RSA (Massimini et al., 2011; Wu and Cavanagh, 1995). Although both methods were performed for the same sequential image pairs, the aforementioned inpainting technique was performed for the 2D–3D method alone. To analyze the accuracy based on anatomical landmarks of the bone, we applied the local coordinate system referencing the International Society of Biomechanics (ISB) 2005 recommendations (Wu et al., 2005) (Supplemental material 1). The mean absolute error (MAE) with standard deviation (SD) and root mean square error (RMSE) in 6 DOF of rotation and translation were compared between the 2D–3D method and RSA in each frame for all 125 frames.

Supplementary data associated with this article can be found, in the online version, at https://doi.org/10.1016/j.jbiomech.2019.04.017.

2.6. Motion analysis comparison of measurements between the 2D–3D and simulated multiple CT methods in a PLRI patient

A 46-year-old male with posttraumatic elbow instability was diagnosed with PLRI on the basis of positive posterolateral rotatory instability test (O'Driscoll et al., 1991). After providing informed consent, a biplane fluoroscopy during forearm rotation was performed for approximately 5 s (60 frames) along with CT at one static position. The radial head motion relative to the humerus was analyzed during forearm rotation when the radial head was dislocated and reduced. The motion of the center of the radial head during forearm rotation was calculated using both the 2D–3D and simulated multiple CT methods. To compare calculations of the same forearm motion by the two methods, five positions were selected from 60 frames obtained by the 2D–3D method (1, 15, 30, 45, and 60), and these five positions from 2D–3D matching were used to perform simulated multiple CT methods. The screw displacement axis or helical axis method (An et al., 1988; Crisco et al., 2001; Panjabi et al., 1981), which describes the spatial movement of a rigid body by rotation around a unique axis and translation along the axis, was adopted for interpolation between two adjacent positions in the simulated multiple CT method. In the screw displacement axis methods, the radius and ulna of the initial frame position were superimposed onto the corresponding bone of the next frame position and the 6 DOF translational matrix was calculated between the positions. Then, a unique axis called screw axis was calculated from the translation matrix and the motions of the bones were described by single rotations around the axis and translations along the axis. The screw displacement axis method has been used for kinematic or motion analyses in several similar studies (Abe et al., 2018; Arimitsu et al., 2009; Miyake et al., 2012; Moritomo et al., 2006; Tay et al., 2008, 2010). The motion of the radial head was compared between the two methods. The coordinate system for the humerus was defined (Supplemental material 2).

2.7. Radiation exposure level for in vivo forearm rotation

Six normal male participants (age, 31–53 years; BMI, 22.0–25.9 kg/m^2) who provided informed consent underwent fluoroscopy and CT to measure radiation exposure level in fluoroscopic test (recorded by C-arm detector) and to determine the CT dose index (CTDI; recorded by CT system).

3. Results

3.1. Phantom motion comparison between the 2D–3D method and RSA

The overall results of trials 1 and 2 indicated that the MAE ± SD for rotation error of the radius and ulna were 0.31 ± 0.35° and 0.32 ± 0.33°, respectively and the translation errors of the radius and ulna were 0.43 ± 0.35 mm and 0.29 ± 0.25 mm, respectively. Additionally, RMSE for rotation of the radius and ulna were 0.47° and 0.46°, respectively and RMSE for translation of the radius and ulna were 0.56 mm and 0.39 mm, respectively. TOST indicated that the 95% CIs of the mean difference between trials 1 and 2 for the radius and ulna were 0.099–0.168 and 0.105–0.162,

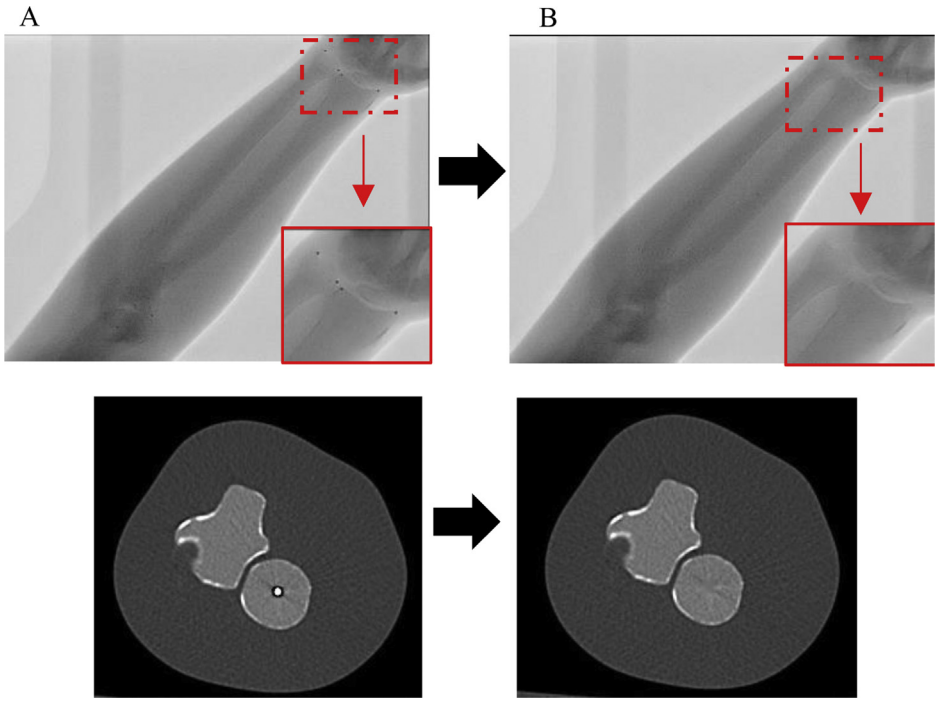

Fig. 3. Fluorography and computed tomography images of the arm phantom (a) before (original) and (b) after the inpainting technique, in which the intensity of the stainless spheres was replaced with the intensity that naturally fused with the image patterns around. Insert shows magnification of stainless steel spheres implanted on anatomical landmarks on the radius and ulna.

respectively. The two trials achieved an accuracy within 0.2 mm/°. The detailed error in each direction is shown in Table 1.

3.2. Comparison of motion analysis between the 2D–3D and simulated multiple CT methods in a PLRI patient

Radial head motion relative to the humerus measured by the two methods is shown in Fig. 4 and Videos 1 and 2. The 2D–3D method but not the simulated multiple CT method detected the quick motion of radial head dislocation and reposition during forearm rotation (Fig. 4). The radial head translated approximately 15 and 8 mm in the posterior and lateral directions when the radial head dislocated within 0.16–0.24 s.

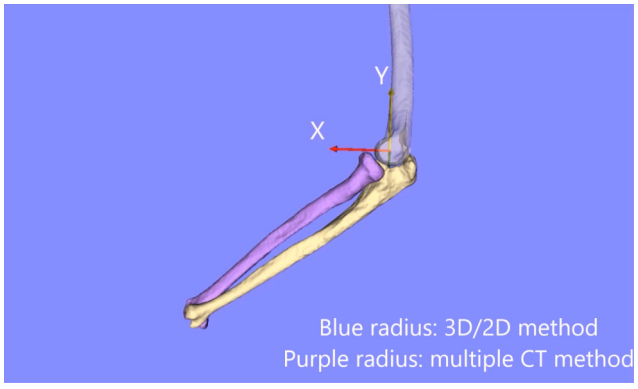

Video 2

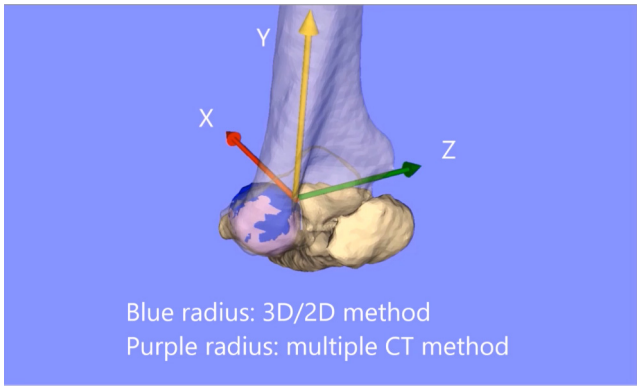

Video 1.

3.3. Radiation exposure for in vivo forearm rotation in the 2D–3D and multiple CT methods

We demonstrated a representative case of the proposed in vivo forearm rotation analysis in Video 3. The radiation exposure for fluoroscopy was 0.23 ± 0.18 mGy, and CTDI was 1.35 mGy for the CT at one static position. The multiple CT method required 4.05 mGy (1.35 × 3 mGy) for CT acquisition at three positions.

4. Discussion

We proposed a biplane fluoroscopic intensity-based 2D–3D matching method for forearm rotational analysis and validated its accuracy and repeatability. This method employed automatic processing and provided high temporal resolution and spatial accuracy, enabling detection of rapid motions (Fig. 4, Videos 1

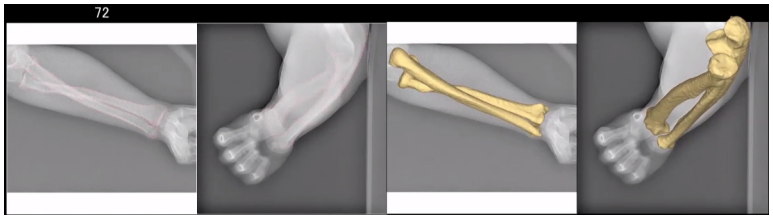

Video 3.

Table 1
Rotation and translation error between the 3D–2D and RSA methods using Euler angles.

Trial 1		Rotation (°)				Translation (mm)			
		Varus–Valgus	Internal rotation–External rotation	Flexion–Extension	Total	Anterior–Posterior	Proximal–Distal	Medial–Lateral	Total
Radius	MAE ± SD	0.73 ± 0.59	0.34 ± 0.26	0.10 ± 0.08	0.39 ± 0.46	0.39 ± 0.33	0.61 ± 0.42	0.50 ± 0.45	0.50 ± 0.41
	RMSE	0.94	0.42	0.13	0.60	0.52	0.74	0.67	0.65
Ulna	MAE ± SD	0.11 ± 0.09	0.41 ± 0.31	0.70 ± 0.56	0.41 ± 0.44	0.40 ± 0.28	0.36 ± 0.26	0.36 ± 0.27	0.37 ± 0.27
	RMSE	0.14	0.51	0.89	0.60	0.49	0.44	0.45	0.46
Trial 2		Rotation (°)				Translation (mm)			
		Varus–Valgus	Internal rotation–External rotation	Flexion–Extension	Total	Anterior–Posterior	Proximal–Distal	Medial–Lateral	Total
Radius	MAE ± SD	0.32 ± 0.27	0.30 ± 0.24	0.13 ± 0.11	0.25 ± 0.23	0.48 ± 0.36	0.34 ± 0.26	0.31 ± 0.23	0.38 ± 0.30
	RMSE	0.42	0.38	0.17	0.34	0.61	0.43	0.39	0.48
Ulna	MAE ± SD	0.33 ± 0.21	0.29 ± 0.19	0.20 ± 0.13	0.27 ± 0.19	0.12 ± 0.09	0.22 ± 0.19	0.38 ± 0.27	0.24 ± 0.22
	RMSE	0.39	0.34	0.23	0.33	0.15	0.29	0.46	0.33

MAE: Mean absolute error.
SD: Standard deviation.
RMSE: Root mean square error.

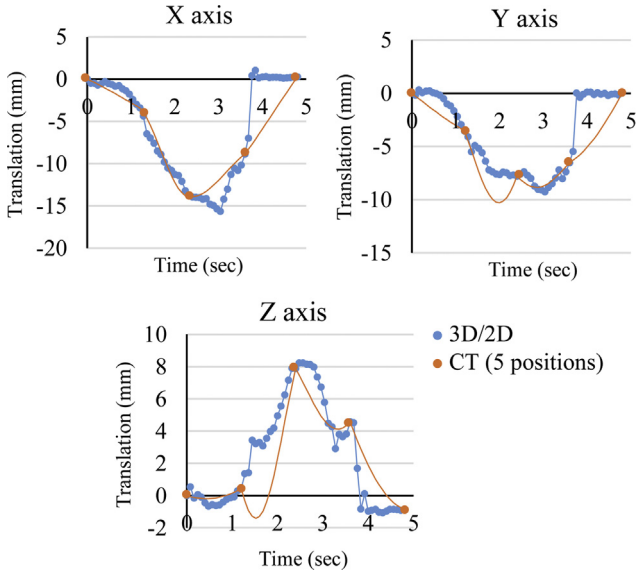

Fig. 4. Motion of the center of the radial head relative to the humerus in a patient with posterolateral rotatory instability using both the 2D–3D and multiple CT methods is shown. The positive X-, Y-, and Z-axes indicate the anterior, proximal, and lateral directions, respectively. The radial head dislocated between 1 and 2 s and reduced just before 4 s. Multiple CT method showed the flexion point because it uses the screw displacement axis method to interpolate between two adjacent positions.

and 2). Radiation exposure in the 2D–3D method was lower than that in the multiple CT method, making the 2D–3D method suitable for practical applications in vivo.

Recently, a four-dimensional CT method (Zhao et al., 2015) for analyzing accurate wrist motion was reported; However, this method increases the radiation dose (36 mGy), and the FOV is limited to small regions (38.4 mm for the longitudinal axis), thereby restricting capture of the entire radius and ulna for forearm motion analysis.

A single-plane fluoroscopic feature-based 2D–3D matching technique using lateral fluoroscopic images for analyzing forearm rotation was reported (Matsuki et al., 2010); however, its accuracy was only compared against knee squat motion analysis. Unlike knee squat motion, forearm rotation comprises more complex 3D motions, including out-of-plane motion from the lateral view. Therefore, forearm rotational analysis using a single-plane 2D image inevitably generates bone overlaps, likely degrading the matching error. Massimini et al. reported ±0.3 mm translation and ±0.5° rotation accuracies for a biplane fluoroscopic feature-based 2D–3D method with manual matching for analyzing shoulder joint elevation (Massimini et al., 2011). Compared with their method, our method uses automatic matching and provides similar accuracy as reported by Massimini et al.

The study has some limitations. First, quantitative validation of accuracy was only performed using a phantom. However, image contrast between cortical bone and soft tissue or cancellous bone was clearer in the human body than in the phantom (Supplemental material 3). Therefore, the accuracy of the 2D–3D method in humans is expected to be equal to or better than that in the phantom. Second, limited FOV of fluoroscopy would restrict the body size analyzed by this method. Finally, the accuracy of motion analysis using biplane fluoroscopic 2D–3D matching is affected by the frame rate, synchrony between the two planes, and motion speed of the objects. In this study, the RSA method was affected by asynchronous biplane images, but we obtained high accuracy under the conditions used (i.e. 12.5 fps and 40°/sec speed motion). We found

that the proposed method could detect joint dislocation or reduction in PLRI patient.

In conclusion, we proposed a new motion analysis method using a biplane fluoroscopic intensity-based 2D–3D matching with high temporal and spatial resolutions, automatic processing, and low radiation exposure. This method would enable 3D forearm rotational motion analysis in real time. PLRI of the elbow can cause bony impingement, leading to early osteoarthritis and bone deficits. The proposed 2D–3D method would uncover the 3D impact point and clarify the mechanism of osteoarthritis progression after PLRI. This technique may further the understanding of joint dislocation or subluxation related to future joint osteoarthritis.

Acknowledgment

The authors would like to thank Hisashi Tanaka, a radiologist, for collaboration on this work. We also thank Yasuhiro Yanagawa and Kazuya Yamaguchi, radiology technologists, for assistance with the experiments. We are grateful to Ryouji Nakao, a computer programmer, for contributing to the study.

This research was supported by MEXT/JSPS KAKENHI 26108004, JST PRESTO 20407, and JSPS KAKENHI 15K10442.

Conflict of interest statement

All authors declare no conflict of interest.

References

Abe, S., Moritomo, H., Oka, K., Sugamoto, K., Kasubuchi, K., Murase, T., Yoshikawa, H., 2018. Three-dimensional kinematics of the lunate, hamate, capitate and triquetrum with type 1 or 2 lunate morphology. J. Hand Surgery 43, 380–386.

Aizawa, J., Masuda, T., Koyama, T., Nakamaru, K., Isozaki, K., Okawa, A., Morita, S., 2010. Three-dimensional motion of the upper extremity joints during various activities of daily living. J. Biomech. 43, 2915–2922.

An, K.N., Jacobsen, M.C., Berglund, L.J., Chao, E.Y., 1988. Application of a magnetic tracking device to kinesiologic studies. J. Biomech. 21, 613–620.

Arimitsu, S., Murase, T., Hashimoto, J., Yoshikawa, H., Sugamoto, K., Moritomo, H., 2009. Three-dimensional kinematics of the rheumatoid wrist after partial arthrodesis. J. Bone Joint Surg. 91, 2180–2187.

Crisco, J.J., Wolfe, S.W., Neu, C.P., Pike, S., 2001. Advances in the in vivo measurement of normal and abnormal carpal kinematics. Orthop. Clinics North Am 32, 219–231.

de Bruin, P.W., Kaptein, B.L., Stoel, B.C., Reiber, J.H., Rozing, P.M., Valstar, E.R., 2008. Image-based RSA: Roentgen stereophotogrammetric analysis based on 2D–3D image registration. J. Biomech. 41, 155–164.

Horn, B.K.P., 1987. Closed-form solution of absolute orientation using unit quaternions. J. Opt. Soc. Am. 4, 629–642.

Hunsche, S., Sauner, D., Majdoub, F.E., Neudorfer, C., Poggenborg, J., Gossmann, A., Maarouf, M., 2017. Intensity-based 2D 3D registration for lead localization in robot guided deep brain stimulation. Phys. Med. Biol. 62, 2417–2426.

Kato, H., Billinghurst, M., 1999. Year Marker tracking and hmd calibration for a video-based augmented reality conferencing system. In: Augmented Reality, 1999. (IWAR'99) Proceedings. 2nd IEEE and ACM International Workshop on 1999.

Li, X., 2011. Image recovery via hybrid sparse representations: a deterministic annealing approach. IEEE J. Sel. Top. Signal Process. 5, 953–962.

Massimini, D.F., Warner, J.J., Li, G., 2011. Non-invasive determination of coupled motion of the scapula and humerus–an in-vitro validation. J. Biomech. 44, 408–412.

Matsuki, K.O., Matsuki, K., Mu, S., Sasho, T., Nakagawa, K., Ochiai, N., Takahashi, K., Banks, S.A., 2010. In vivo 3D kinematics of normal forearms: analysis of dynamic forearm rotation. Clin. Biomech. 25, 979–983.

Miyake, J., Moritomo, H., Kataoka, T., Murase, T., Sugamoto, K., 2012. In vivo three-dimensional motion analysis of chronic radial head dislocations. Clin. Orthop. Relat. Res. 470, 2746–2755.

Moritomo, H., Murase, T., Goto, A., Oka, K., Sugamoto, K., Yoshikawa, H., 2006. In vivo three-dimensional kinematics of the midcarpal joint of the wrist. J. Bone Joint Surg. 88, 611–621.

Morrey, B.F., Askew, L.J., Chao, E.Y., 1981. A biomechanical study of normal functional elbow motion. J. Bone Joint Surg. 63, 872–877.

O'Driscoll, S.W., Bell, D.F., Morrey, B.F., 1991. Posterolateral rotatory instability of the elbow. J. Bone Joint Surg. 73, 440–446.

Oka, K., Murase, T., Moritomo, H., Goto, A., Sugamoto, K., Yoshikawa, H., 2009. Accuracy analysis of three-dimensional bone surface models of the forearm constructed from multidetector computed tomography data. Int. J. Med. Robot. 5, 452–457.

Omori, S., Miyake, J., Oka, K., Tanaka, H., Yoshikawa, H., Murase, T., 2016. In vivo three-dimensional elbow biomechanics during forearm rotation. J. Shoulder Elbow Surg. 25, 112–119.

Otake, Y., Wang, A.S., Webster Stayman, J., Uneri, A., Kleinszig, G., Vogt, S., Khanna, A.J., Gokaslan, Z.L., Siewerdsen, J.H., 2013. Robust 3D–2D image registration: application to spine interventions and vertebral labeling in the presence of anatomical deformation. Phys. Med. Biol. 58, 8535–8553.

Panjabi, M.M., Krag, M.H., Goel, V.K., 1981. A technique for measurement and description of three-dimensional six degree-of-freedom motion of a body joint with an application to the human spine. J. Biomech. 14, 447–460.

Stiehl, J.B., Dennis, D.A., Komistek, R.D., Keblish, P.A., 1997. In vivo kinematic analysis of a mobile bearing total knee prosthesis. Clin. Orthop. Relat. Res., 60–66

Tay, S.C., van Riet, R., Kazunari, T., Amrami, K.K., An, K.N., Berger, R.A., 2010. In-vivo kinematic analysis of forearm rotation using helical axis analysis. Clin. Biomech. 25, 655–659.

Tay, S.C., van Riet, R., Kazunari, T., Koff, M.F., Amrami, K.K., An, K.N., Berger, R.A., 2008. A method for in-vivo kinematic analysis of the forearm. J. Biomech. 41, 56–62.

Wu, G., Cavanagh, P.R., 1995. ISB recommendations for standardization in the reporting of kinematic data. J. Biomech. 28, 1257–1261.

Wu, G., van der Helm, F.C.T., Veeger, H.E.J., Makhsous, M., Van Roy, P., Anglin, C., Nagels, J., Karduna, A.R., McQuade, K., Wang, X., Werner, F.W., Buchholz, B., 2005. ISB recommendation on definitions of joint coordinate systems of various joints for the reporting of human joint motion—Part II: shoulder, elbow, wrist and hand. J. Biomech. 38, 981–992.

Zhao, K., Breighner, R., Holmes 3rd, D., Leng, S., McCollough, C., An, K.N., 2015. A technique for quantifying wrist motion using four-dimensional computed tomography: approach and validation. J. Biomech. Eng. 137.

Zhu, Z., Massimini, D.F., Wang, G., Warner, J.J., Li, G., 2012. The accuracy and repeatability of an automatic 2D–3D fluoroscopic image-model registration technique for determining shoulder joint kinematics. Med. Eng. Phys. 34, 1303–1309.